

## Chapter 1

# Elements of nuclear structure

### 1.1 Introduction

A nucleus is the core of an atom. By atomic standards, its dimensions are minuscule. Atoms have radii of the order of  $10^{-9}\text{m}$  whereas nuclear radii are more like  $10^{-14}\text{m}$ . Compared to an atom, a nucleus is like a grain of sand in a football stadium. Nevertheless, its mass is almost the entire mass of the atom. Approximately 99.97% of the mass of an atom resides in its nucleus. This means that, by mass, approximately 99.97% of the material world is nuclear matter.

Nuclei consist of nucleons of which there are two types: positively charged protons and uncharged neutrons. Both nucleon types have essentially the same mass and are approximately 2000 times as massive as an electron. They are held together in a nucleus by the so-called *strong interaction*. This interaction is much stronger but of much shorter range than the Coulomb interaction that binds the atomic electrons to their nuclei. At a separation distance of 1.0 fm, the strong attraction between two nucleons is some 30 times as strong as the Coulomb repulsion between two protons. However, at a distance of 20 fm, the strong interaction is smaller than the Coulomb interaction by a factor of 2000.

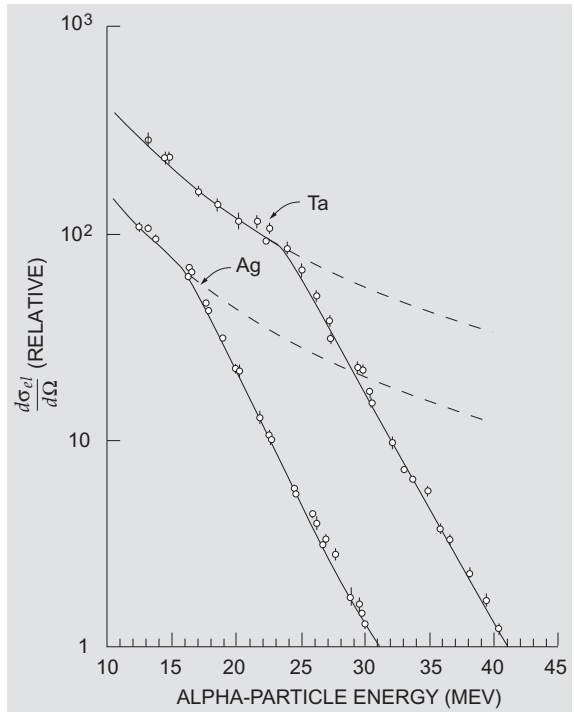
In spite of the predominance of nuclear matter in our world, it is easy to be oblivious to the existence of nuclei. This is because nuclei are hidden beneath protective clouds of atomic electrons which effectively keep them apart. In addition, nuclei are prevented from coming into contact with one another by the electrostatic repulsions that result from their positive charges. Thus, one has little direct experience of nuclei outside of the nuclear physics laboratory.

Because nuclei are so isolated, it is not surprising that most physical properties of the everyday world can be explained in terms of atoms and the electronic bonds they make with one another to form molecules and solids. Nevertheless, to understand the existence of atoms, one must first understand the existence of nuclei. Indeed, since an atom is stable only if its nucleus is stable, the question of which atoms can exist is one of nuclear physics. So also is the issue of how many chemical elements are accessible for use or study. At an even more fundamental level, the question of how atoms come into being at all is one of nuclear physics.

Nuclei are created in stars where the temperatures are literally astronomical. Such temperatures are necessary because nuclear reactions occur on an energy scale of hundreds of keV and room temperature corresponds only to an energy of 1/40 eV. Thus, for a nucleus, room temperature might just as well be at absolute zero. A nucleus at room temperature is very cold. It only starts to become “warm” at temperatures of one billion Kelvin. If such temperatures were not approached in stars, the rich variety of nuclei and the atoms they inhabit would not have materialised.

The nucleus was discovered by Geiger and Marsden<sup>1,2</sup> using a beam of alpha particles emitted by radioactive radium daughter nuclei. Geiger and Marsden directed an alpha particle beam at thin metal foils and to their surprise, observed some of the alpha particles to be scattered to large backward angles. From these experiments Rutherford<sup>3</sup> was able to infer the existence of the nucleus and an upper limit on its size. Figure 1.1 shows differential cross sections, as a function of bom-

Figure 1.1: Differential cross sections for the elastic scattering of alpha particles from silver ( $Z = 47$ ) and tantalum ( $Z = 73$ ) as a function of bombarding energy observed at an angle of  $60^\circ$ . The dashed curves are the theoretical (Rutherford) cross sections for scattering alpha particles by a point charge distribution. These curves agree well with the data at low energies. The sudden departures from these curves that occur when the alpha particles have sufficient energy to come into contact with the nucleus provide a measure of the corresponding nuclear size. (The figure is from Eisberg R.M. and Porter C.E. (1961), *Rev. Mod. Phys.* **33**, 190.)



barding energy, for the scattering of alpha particles from silver and tantalum. At low energies, the results are similar to those obtained by Geiger and Marsden and are in excellent agreement with the so-called *Rutherford cross section*. Rutherford’s

<sup>1</sup>Geiger H. and Marsden E. (1909), *Proc. Roy. Soc. London* **A82**, 495.

<sup>2</sup>Geiger H. (1910), *Proc. Roy. Soc. London* **A83**, 492.

<sup>3</sup>Rutherford E. (1911), *Phil. Mag.* **21**, 669.

cross section is what one expects if the alpha particles don't come into contact with the nucleus, i.e., if the scattering results purely from the long-range Coulomb interaction. Thus, the energy at which the cross section suddenly departs from the Rutherford curve (not seen by Geiger and Marsden but seen at the higher energies shown in Figure 1.1) provides a measure of the size of the corresponding nucleus.

Twentieth century science and technology have caused nuclear physics to impact on everyday life in a variety of ways. Some examples are: uses of nuclear radiation in such diverse areas as materials characterisation and cancer therapy; the uses of radioactive isotopes as tracers and diagnostic tools in medicine; nuclear magnetic resonance and positron emission tomography for medical imaging; uses of nuclear accelerators as spectrometers for carbon dating and the detection of rare trace elements (and to produce sources of nuclear radiation); nuclear fission in nuclear power reactors and nuclear weapons; and nuclear fusion in weapons and in the development of fusion reactors for our future energy needs.

To date, 117 chemical elements have been identified. Each element is characterised by an atom with a specified number,  $Z$ , of electrons and a nucleus with an equal number of protons. However, an element may have more than one isotopic form. An isotope is characterised by a nucleus with proton number  $Z$  and neutron number  $N$ . Approximately 2800 isotopes have been identified. They are shown in Figure 1.2. A total of 7000 are believed to be sufficiently long-lived for their identification to be possible with current techniques. However, the less stable nuclei have not yet been produced in sufficient numbers for experimental investigation.

Figure 1.2 also shows the approximate limits to the region of observable nuclei. Nuclei for which the binding energy of the last neutron,  $B_n$ , is negative are excluded. Nuclei for which the binding energy of the last proton,  $B_p$ , is insufficient to delay tunnelling through the Coulomb barrier by more than  $\sim 10$  ns are also excluded. Figure 1.3 shows examples of  $(N, Z)$  combinations for which these limits have been reached.

In this introductory chapter, we present a summary of the important facets of nuclear structure illustrated liberally with experimental data. We also include elementary quantum mechanical descriptions of the two most important models of nuclear structure: the shell model (which explains the magic numbers) and the collective model.

The chapter is relatively self-contained and can be read on its own. Its purpose is to lay the phenomenological foundations of nuclear physics. We shall attempt to show that interpretations of nuclear phenomena often emerge naturally from a systematic examination of the data. To this end, we present the best and most up-to-date data that we could find rather than the data which constituted the original evidence. Details of the models and their implications for understanding the nuclear many-body problem are developed in subsequent chapters.

A phenomenological approach to nuclear structure physics is appropriate because there is no *a priori* theory which could have predicted the properties of nuclei

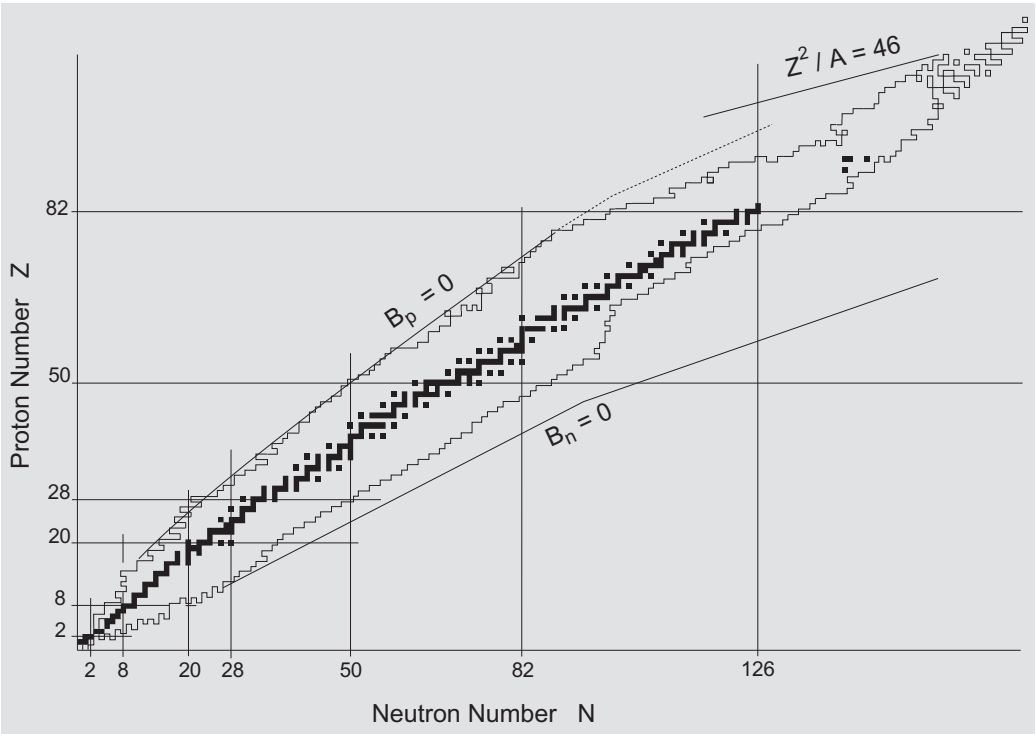


Figure 1.2: Chart of the nuclides (ca. 2005). The black squares denote the nuclei found in nature. The present extent of nuclei, for which at least one characteristic has been measured, are enclosed by the “stepped” border. The line marked  $B_n = 0$  approximates the neutron drip line. The line marked  $B_p = 0$  approximates the proton drip line. Outside of these borders, neutrons and protons are lost so rapidly from nuclei that the nuclei cannot be observed. The line marked  $Z^2/A = 46$  indicates an approximate limit to nuclear stability with respect to spontaneous fission. The magic numbers 2, 8, 20, 28, 50, 82, and 126 (cf. Section 1.3) also are indicated.

before they were observed. There have been many experimental surprises. In this respect, nuclear physics is in “good company” with condensed matter physics. There are a number of parallels. For example, many nuclei and condensed matter systems exhibit superfluidity. In fact, it is sensible to regard nuclei as examples of condensed matter.

The future of nuclear physics, as also of condensed matter physics, depends in part on producing new condensates. For nuclei this means new combinations of  $N$  and  $Z$ . A consideration of Figure 1.2 reveals that we have studied only about 30% of the possibilities. To study the remaining 70% of the possibilities, which are very unstable, is one of the future challenges of nuclear physics.

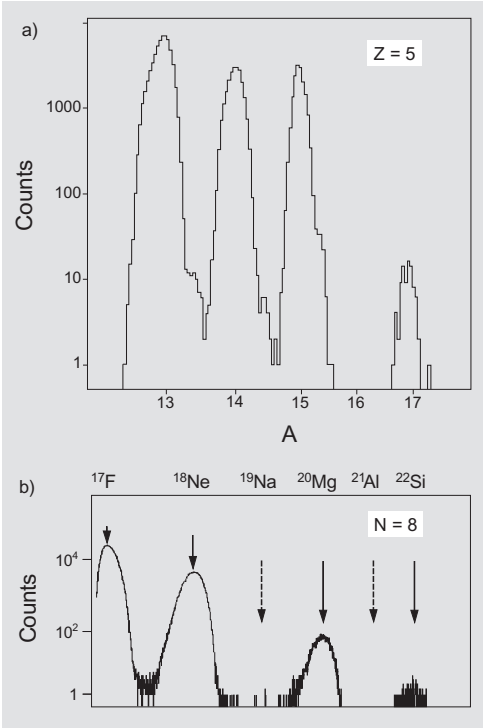


Figure 1.3: (a) Mass spectrum of fragments with  $Z = 5$  (boron isotopes), following the bombardment of a tantalum target with a 1760 MeV beam of  $^{40}\text{Ar}$  ions (Langevin M. *et al.* (1985), *Phys. Lett. B* **150**, 71). Evidently,  $^{16}_5\text{B}$  either does not exist or is too short lived to reach the detector system. (b) Mass spectrum of fragments with  $N = 8$  in a similar nuclear reaction to (a) (Saint-Laurent M.G. *et al.* (1987), *Phys. Rev. Lett.* **59**, 33). Both  $^{19}\text{Na}$  and  $^{21}\text{Al}$  are absent, again implying either that they do not exist, or that they decay (e.g., by proton tunnelling through the Coulomb barrier) too quickly to be observed.

### Exercises

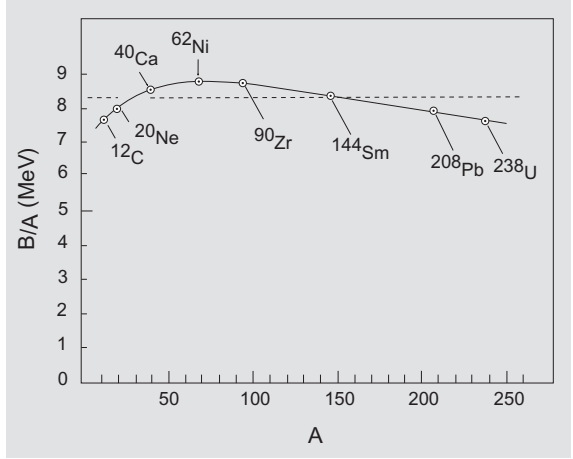
- 1.1 Using  $F_{\text{Coulomb}} = \frac{q_1 q_2}{4\pi\epsilon_0 r^2}$  where  $\epsilon_0 = 8.85 \times 10^{-12} \text{ C}^2\text{m}^{-2}\text{N}^{-1}$ , and  $F_{\text{Yukawa}} = -\frac{d}{dr} \left( \frac{V_0 e^{-\lambda r}}{\lambda r} \right)$  where  $V_0 = -40 \text{ MeV}$  and  $\lambda = 0.7 \text{ fm}^{-1}$ , calculate the magnitudes of  $F_{\text{Coulomb}}$  and  $F_{\text{Yukawa}}$  at 1.0 and 20 fm. (The Yukawa force is an approximation to the strong interaction between two nucleons (cf. Section 5.7)).
- 1.2 Use Figure 1.1 to estimate the radii (in fm) of silver and tantalum nuclei. Assume  $R(^4\text{He}) = 1.7 \text{ fm}$  and a range of 1.4 fm for the strong interaction.

## 1.2 Nuclear structure from gross properties

A first look at the gross properties of nuclei (e.g., binding energies, radii, and densities) suggests that they have many properties in common with liquid drops. They have binding energies and volumes that increase more or less linearly with nucleon number and they have densities that approach a saturation value at the centres of all but the lightest nuclei (cf. Figure 1.7).

The binding energy per nucleon,  $B/A$ , as a function of  $A$  ( $= Z + N$ ) is shown in Figure 1.4. From  $A \approx 20$  to  $A \approx 200$  it has the approximately constant value of 8.3 MeV/nucleon. This near constancy (to within  $\pm 5\%$ ) indicates that the range of the nucleon-nucleon force is short compared to the size of the nucleus. A short-range

Figure 1.4: A plot of binding energy per nucleon,  $B/A$ , versus mass number  $A$ . The quantities  $B/A$  are experimental. Over the mass range  $20 \leq A \leq 200$ , the average value of  $B/A$  is  $\sim 8.3$  MeV/nucleon (the horizontal dashed line). The most tightly bound nucleus is  $^{62}\text{Ni}$  which has a binding energy of 8.795 MeV/nucleon. The solid curve is a smooth line through the data. The data points, for the nuclei shown, are chosen arbitrarily. (The data are from Audi G., Wapstra A.H. and Thibault C. (2003), *Nucl. Phys.* **A729**, 337.)



force between particles in a many-body system only acts between near neighbours. Thus, for a large nucleus, the binding energy per nucleon is independent of nuclear volume. However, for finite nuclei, there are surface effects; nucleons at the surface do not have a full contingent of neighbours. This is reflected in the decrease of  $B/A$  for light nuclei which have a larger fraction of their nucleons at the surface. In contrast, a long-range force between nucleons would result in a non-constant value of  $B/A$ . The Coulomb repulsion between protons in nuclei is of this type. It causes the decrease of  $B/A$  for heavy nuclei and ultimately limits the stability of very heavy nuclei. The practical consequence of this is spontaneous fission, as would occur for a droplet of water if an increasing electrostatic charge were applied. The  $Z^2/A = 46$  line, beyond which spontaneous fission half-lives are estimated to be less than  $1 \mu\text{s}$ , is shown in Figure 1.2. Another consequence of the Coulomb force in nuclei is the curvature of the stability line, evident in Figure 1.2, towards neutron excess in heavy nuclei.

Nuclear charge distributions are probed, for example, in electron scattering experiments. Nuclear mass radii are less easily measured. However, it is generally assumed that, with the exception of a few neutron-rich nuclei such as  $^7_3\text{Li}$ , the nuclear mass and charge distributions are proportional to one another.

Root-mean-square charge radii are shown as a function of  $A^{1/3}$ , for selected nuclei, in Figure 1.5. For heavy nuclei, the data approximate the straight line with

$$\left[ \frac{5}{3} \langle r^2 \rangle_{\text{expt}} \right]^{\frac{1}{2}} \approx 1.1 A^{1/3} + 0.65 \text{ fm}. \quad (1.1)$$

The factor  $\frac{5}{3}$  is included in this expression because, for constant-density matter with a sharply-defined surface of radius  $r = R_0 A^{1/3}$  (cf. Figure 1.6), the mean-square radius would be given by

$$\langle r^2 \rangle = \frac{3}{5} R_0^2 A^{2/3}. \quad (1.2)$$

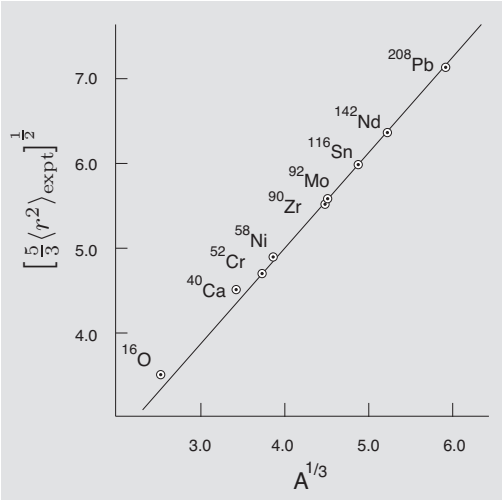


Figure 1.5: A plot of the root-mean-square charge radius,  $[\frac{5}{3}\langle r^2 \rangle_{\text{expt}}]^{1/2}$ , versus  $A^{1/3}$ . Data are for selected nuclei. The solid line is a best (straight-line) fit for nuclei with  $A \geq 90$ . The deviation of the lighter nuclei from this line is due to surface diffuseness effects (cf. Figure 1.7). The units are femtometres (1 fm =  $10^{-15}$  m). (The data are from Angeli I. (2004), *At. Data Nucl. Data Tables* **87**, 185.)

Thus, the data indicate that the charge density of nuclear matter is essentially constant in heavy nuclei. Variations from Equation (1.2) in light nuclei can be attributed to surface effects (cf. Figure 1.7).

Taken together, Figures 1.4 and 1.5 suggest that nuclear matter resembles a liquid and that nuclei can be modelled as liquid drops. Indeed, a liquid-drop model of the nucleus is quite successful at describing many gross properties of nuclei. However, whereas classical liquid drops have sharply defined surfaces, the nuclear density distribution has a diffuse surface. This is revealed by electron scattering cross sections as depicted, for  $^{197}\text{Au}$ , in Figure 1.6. The cross section shown is fitted accurately by the expression for the nuclear charge density

$$\rho(r) = \rho_0 \left\{ 1 + \exp\left(\frac{r - R_B}{a}\right) \right\}^{-1}, \quad (1.3)$$

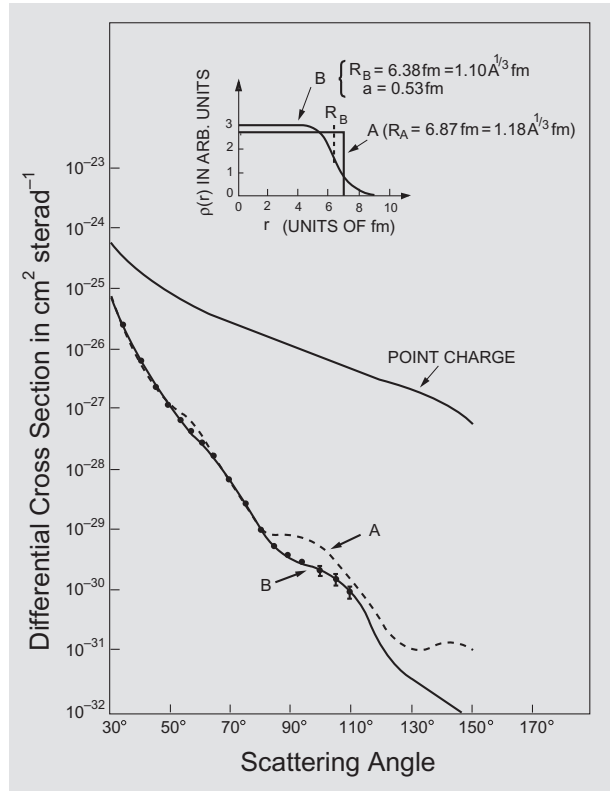
where  $\rho_0$  is the central density,  $R_B$  is the radius at half density and  $a$  is a surface diffuseness parameter. Figure 1.7 shows the variation in nuclear charge density as a function of mass number.

The decreasing saturation density with increasing  $Z$  is a Coulomb repulsion effect.

### Exercises

- 1.3 Derive the factor  $\frac{3}{5}$  in Equation (1.2).
- 1.4 For a long-range force in a finite  $A$ -body system, show that the binding energy  $B \propto A(A - 1)$ .
- 1.5 Using Equation (1.3) with  $R_B = 6.38$  fm,  $a = 0.53$  fm, determine the value of  $r$  for which  $\rho = 0.1\rho_0$ .

Figure 1.6: Differential cross section for elastic scattering of 153 MeV electrons by  $^{197}\text{Au}$  nuclei. The diffraction pattern seen for the differential cross section as a function of angle reveals that the nucleus has a diffuse surface (B) rather than a sharp surface (A). A consequence of this (as shown in the inset) is that the nuclear radius at the half density is slightly smaller than it would be for a nuclear density with a sharp surface that gives the same  $\langle r^2 \rangle^{1/2}$ . The pattern that would be seen for scattering from a point charge is also shown (cf. Figure 1.1). (The figure is from Bohr A. and Mottelson B.R. (1969), *Nuclear Structure*, Vol. 1 (Benjamin, New York), (republished by World Scientific, Singapore), p. 159. The data are from: Hahn B., Ravenhall D.G. and Hofstadter R. (1956), *Phys. Rev.* **101**, 1131; Yennie D.R., Ravenhall D.G. and Wilson R.N. (1954), *Phys. Rev.* **95**, 500; and Herman R. and Hofstadter R. (1960), *High Energy Electron Scattering Tables*, Stanford Univ. Press, Stanford, California.)



### 1.3 Nuclear shell structure

One of the big surprises in the development of nuclear physics was that nuclei, like atoms, exhibit properties characteristic of a system with a shell structure. The origin of shell structure in atoms is well understood. Atomic electrons move in the central (spherically symmetric) Coulomb field of a small, but relatively massive, and highly-charged nucleus. The field of the nucleus, as seen by an electron, is partially screened by other atomic electrons. But, apart from the screening effect, the interactions between electrons are relatively weak. Thus, to a first approximation, an atom can be regarded as a system of independent electrons moving in a partially-screened Coulomb field. Corrections can be made to include the correlation effects induced by the small, but well understood, residual electronic interactions and, with a sufficiently large computer, remarkably accurate results for atomic properties can be computed. The result is that atomic electrons occupy rather well-defined single-particle states. Furthermore, since electrons are spin-half fermions subject to the Pauli exclusion principle, at most two electrons (one spin up and one spin down) can occupy the same spatial state. Thus, in the ground state of an atom, the electrons fill the lowest energy states available. Shell structure arises because the energies of

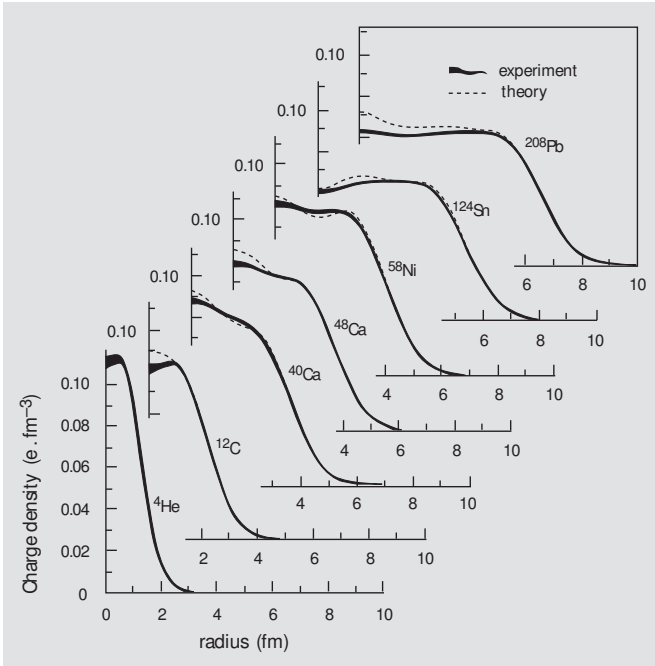


Figure 1.7: Ground-state charge densities for a range of nuclei obtained from elastic electron scattering cross sections. The experimental uncertainties are indicated by the thickness of the lines. The dashed curves are the results of independent-particle model calculations. (The figure shown here, with permission of Bernard Frois, is similar to one appearing in Frois B. and Papanicolas C. (1987), *Ann. Rev. Nucl. Part. Sci.* **37**, 133.)

states are grouped together into “shells” with energy gaps between them.

Shell structure in nuclei is more difficult to understand. A nucleus is composed of neutrons and protons which, like electrons, are spin-half fermions. But, apart from this common feature, atoms and nuclei are very different. Whereas atomic electrons move in the central field of the nucleus, the central field in which nucleons move is self generated. Atomic electrons are far apart and interact weakly by long-range forces. Nucleons inside a nucleus are close to one another and interact strongly by short-range forces. Consequently, the observation of shell structure in nuclei was not expected. Indeed, the interpretation of experimental data in shell-model terms was strongly resisted for many years. The success of the shell model was subsequently attributed to the Pauli exclusion principle which, to a large extent, inhibits the strong scattering of nucleons inside the nucleus by preventing nucleons from scattering into orbitals that are already occupied.

Nuclear shell effects are dominant features of nuclear structure. They lead directly to the nuclear shell model. The shell model is of fundamental importance because it provides the most detailed theoretical framework available for the description of nuclei in terms of interacting nucleons. One of the major aims in developing models and theories of nuclear structure is, therefore, to relate successful models to the shell model. If a model can be expressed in shell-model terms, one is justified in calling the model a *microscopic model*. Moreover, if a model description of some phenomena is successful and the model can be expressed in shell-model terms, one

can claim to have explained the phenomena in terms of interacting neutrons and protons. This is a primary objective of nuclear physics research.

### 1.3.1 Differences in binding energies and radii

Important indicators of nuclear shell structure come from binding-energy differences. Binding-energy differences between neighbouring nuclei are called *separation energies*. One-neutron separation energies are defined by the expression

$$S_n(A, Z) = B(A, Z) - B(A - 1, Z), \quad (1.4)$$

where  $B(A, Z)$  is the binding energy of the nucleus with  $A$  nucleons and  $Z$  protons. Two-neutron separation energies are defined by

$$S_{2n}(A, Z) = B(A, Z) - B(A - 2, Z). \quad (1.5)$$

Proton separation energies are defined in a similar way.

Figure 1.8 shows the one-neutron separation energies for the calcium isotopes. This figure has two striking features. The first is the saw-tooth nature of the plot.

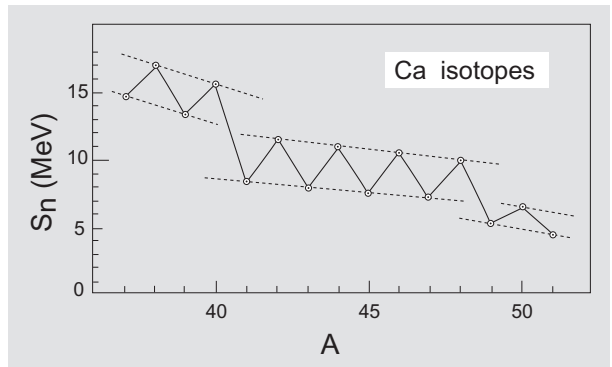


Figure 1.8: One-neutron separation energies,  $S_n$ , for the calcium isotopes. Note the odd-even staggering between neighbouring nuclei and the strong discontinuities that occur between  $A = 40$  and  $41$  and between  $A = 48$  and  $49$  (cf. Figure 1.9). (The data are from Audi G., Wapstra A.H. and Thibault C. (2003), *Nucl. Phys.* **A729**, 337.)

The second is the discontinuities that occur between  $A = 40$  and  $41$  and between  $A = 48$  and  $49$ . The saw-tooth behaviour shows that it requires more energy to remove a neutron when the neutron number is initially even than when it is odd. This odd-even staggering effect is a manifestation of the predisposition of nucleons to form strongly-coupled pairs (cf. comments below and in Section 1.4). Thus, to remove a nucleon from an even nucleus, one has first to break apart the pair to which it belongs and this demands additional energy. The discontinuities at  $A \approx 40$  and  $48$  are indicators of nuclear shell closures. They show up even more clearly in two-neutron separation energies.

Figure 1.9 shows the two-neutron separation energies for the ( $Z = 20$ ) calcium isotopes. The odd-even staggering is now smoothed out but the discontinuities at  $A = 40$  ( $N = 20$ ) and  $48$  ( $N = 28$ ) remain. One sees that it requires significantly

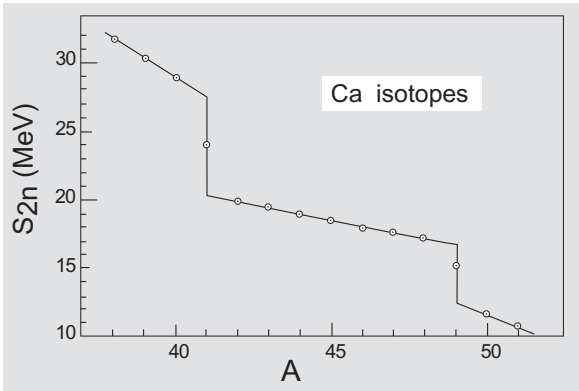


Figure 1.9: Two-neutron separation energies,  $S_{2n}$ , for the calcium isotopes. The odd-even staggering is smoothed away, leaving a clear indication of discontinuities at  $A = 41$  and  $49$ . (The data are from Audi G., Wapstra A.H. and Thibault C. (2003), *Nucl. Phys.* **A729**, 337.)

more energy to remove a pair of neutrons when  $N \leq 20$  than when  $N \geq 22$ .<sup>4</sup> Thus, we say that the discontinuities occur at  $N = 20$  and  $N = 28$ . Such discontinuities are observed both for protons and neutrons at  $N, Z = 2, 8, 20, 28, 50, \text{ and } 82$ , and at  $N = 126$ . Examples of these discontinuities for  $18 \leq N \leq 156$  are shown in Figure 1.10.

Differences in radii between neighbouring isotopes also change dramatically at  $N = 2, 8, 20, 28, 50, 82, \text{ and } 126$ . This is shown for  $24 \leq N \leq 144$  in Figure 1.11. One sees that the differences in radii increase from values close to local minima to values close to local maxima at the specified values of  $N$ . The numbers 2, 8, 20, 28, 50, 82 and 126 are called *magic numbers*. The occurrence of magic numbers suggests a shell structure in nuclei similar to that seen in atoms.

Atoms exhibit changes in binding energies (ionization potentials) and radii (covalent and ionic radii) due to changes in electronic shell filling. When atomic shell filling in atoms passes through the numbers 2, 10, 18, 36, 54, or 86, there are sudden decreases in ionization potentials and sudden increases in covalent and ionic radii. These changes reflect the exclusion of electrons from the “smaller” more strongly-bound configurations that are filled first in atoms. The implication of the data shown in Figures 1.10 and 1.11 is that nuclei also possess shell structure. In atoms, energy shells reflect the dominance of the independent-particle component of the Hamiltonian. A suggestion that the nuclear Hamiltonian contains a dominant independent-particle component, also comes from the observation that magic numbers have the same values for protons and neutrons, regardless of mass number, i.e., magic numbers for protons do not depend on the number of neutrons and vice versa. It is also suggested by the observation of *single-particle* states in the near neighbours of doubly closed-shell nuclei. These are states which, to a first approximation, are simple (uncorrelated) products of core states and single-particle states.

<sup>4</sup>The separation energy of a pair at  $N = 21$  is approximately the average of the  $N = 20$  and  $N = 22$  values. This corresponds to the fact that the first neutron is removed from the  $N = 21$  nucleus and the second from the  $N = 20$  nucleus; the calcium isotopes have  $Z = 20$ .

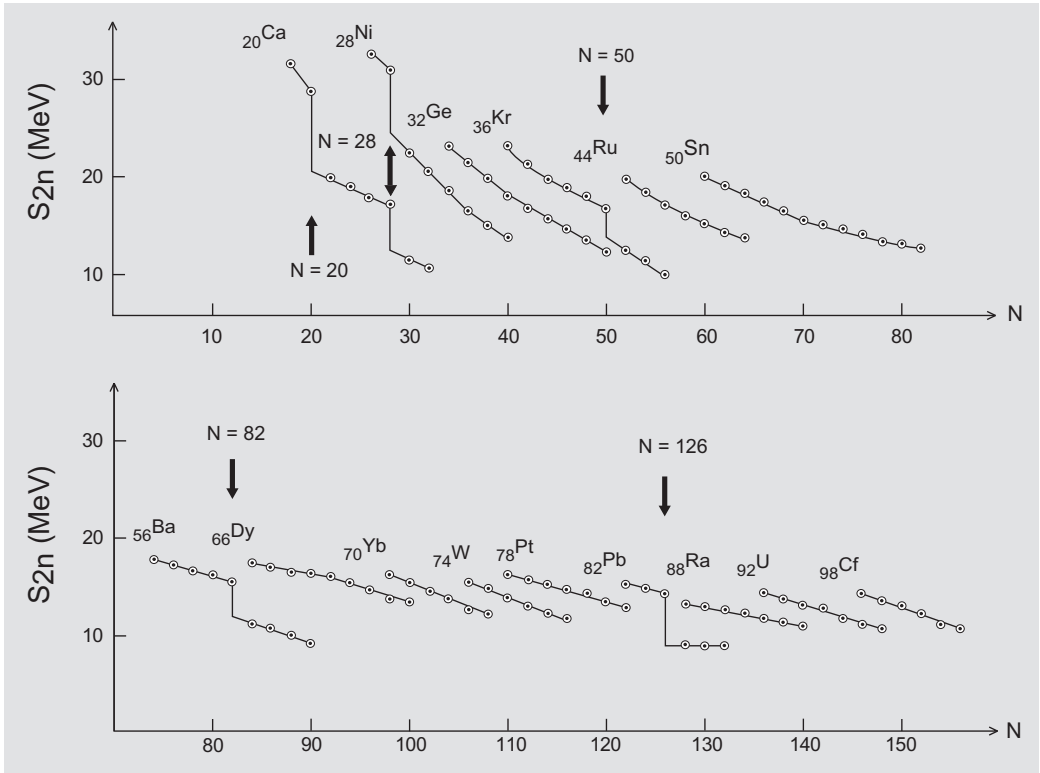


Figure 1.10: Two-neutron separation energies for selected isotopes with even  $N$  from  $Z = 20$  (calcium) to  $Z = 98$  (californium). The energy gaps at  $N = 20, 28, 50, 82$  and  $126$  are clearly visible. Further, there is no evidence for large energy gaps at any other values of  $N$  between 20 and 156. (The data are from Audi G., Wapstra A.H. and Thibault C. (2003), *Nucl. Phys.* **A729**, 337.)

### 1.3.2 Nucleon transfer reactions and spectroscopy

A simple way to identify single-particle states in a nucleus is by means of single-nucleon transfer reactions. A transfer reaction is an interaction between a projectile nucleus and a target nucleus which results in a transfer of nucleons between the two. In a *pickup* reaction, nucleons are removed from the target and added to the projectile whereas in a *stripping* reaction the converse occurs. Transfer reactions are important sources of nuclear structure information because they measure the extent to which a final state of a nucleus differs from an initial state of a neighbouring nucleus by either the addition or removal of one or more nucleons.

Single-nucleon pickup and stripping reactions are particularly important because they enable one to infer the occupation probabilities of single-nucleon states. In an independent-particle model, single-nucleon states are either occupied or empty. However, due to correlations brought about by residual interactions, single-nucleon

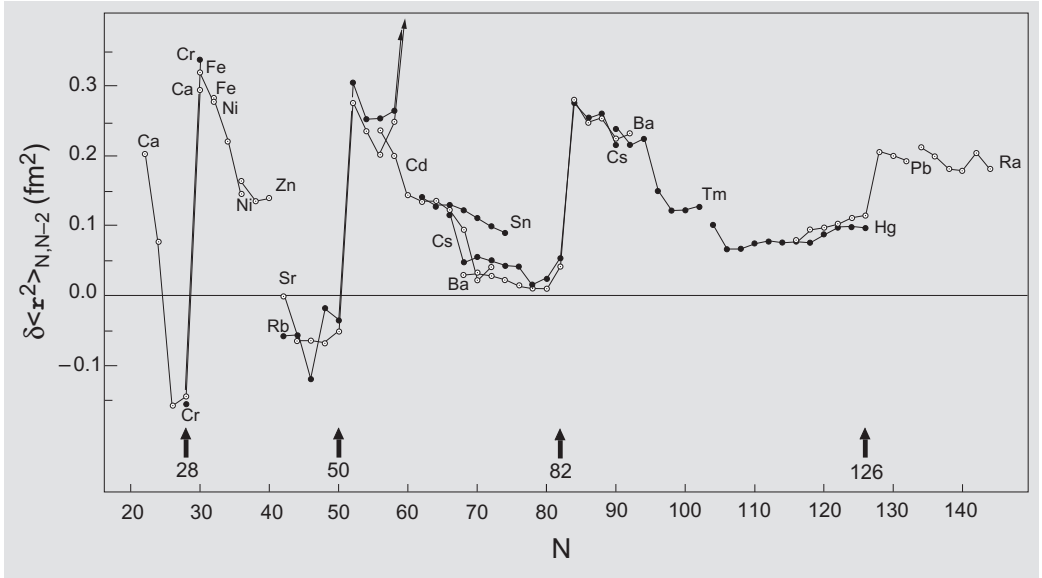


Figure 1.11: Differences in mean-square charge radii for isotopes differing in  $N$  by 2. Data are for selected isotopes and even  $N$ . Solid and open circles are used only to help distinguish isotopic sequences. Discontinuities are clearly evident at  $N = 28, 50, 82,$  and  $126$ . The very large (off-scale) shifts for Rb and Sr at  $N = 60$  are due to a sudden onset of deformation (see Figure 1.41). (The data are from: Otten E.W. (1989), in *Treatise on Heavy-Ion Science, Nuclei Far from Stability*, Vol. 8, edited by D.A. Bromley (Plenum Press, New York), p. 517; Nadjakov E.G., Marinova K.P. and Gangrsky Y.P. (1994), *At. Data Nucl. Data Tables* **56**, 133; Shera E.B. *et al.* (1976), *Phys. Rev.* **C14**, 731 – Fe, Ni, Zn; Mårtensson-Pendrill A.-M. *et al.* (1992), *Phys. Rev.* **A45**, 4675 – Ca; Wendt K. *et al.* (1988), *Z. Phys.* **A329**, 407 – Ba; and Alkhazov G.D. *et al.* (1988), *Nucl. Phys.* **A477**, 37 – Tm.)

states are, in general, fractionally occupied. Thus, to the extent that a single-nucleon state is occupied, it can give up a nucleon in a pickup reaction leaving behind a residual nucleus in a *hole state*. Conversely, to the extent that a single-nucleon state is empty, it can accept a nucleon in a stripping reaction thereby creating a residual nucleus in a *particle state*.

Transfer reactions are simplest to interpret when either the initial or the final state of the target nucleus has spin (i.e., total angular momentum) zero and when the conditions are such that the transition from the initial to the final state occurs, to a good approximation, in a single step. This happens when the interaction between the projectile and target nucleus is weak and can be treated in first order perturbation theory, i.e., in the Born approximation. One then describes the reaction as a *direct reaction*.

When either the state of the target nucleus or the state of the final nucleus has spin zero, the spin and parity of the transferred nucleon in a direct single-nucleon transfer reaction is simply the difference in the spin and parity of the initial and final nuclear states. Moreover, the orbital component of the total angular

momentum of the transferred nucleon can be inferred from the angular distribution of the outgoing ejectiles. Thus, one can obtain information about the state of the transferred nucleon in a direct pickup or stripping reaction.

To study single-particle states in a particular nucleus it is necessary to select a specific target and a suitable projectile. The events corresponding to the reaction of interest are selected by identifying the outgoing ejectile nucleus using charge and mass selection with a magnetic spectrometer. Ejectile nuclei, so-analysed are detected in the focal plane of the spectrometer using, for example, a plate coated with photographic emulsion. Ejectile nuclei with different energies are focused at different positions on the plate by the magnetic spectrometer. The different energies of the ejectile nuclei reflect the energies of the states in the residual nucleus provided that the incident projectile nuclei are monoenergetic.

An example of data obtained in a single-proton stripping reaction is presented in Figure 1.12. In this example the target is  $^{208}\text{Pb}_{126}$ , the projectile is  $^3\text{He}$ , the ejectile is a deuteron ( $^2\text{H}_1$  or d), and the nucleus under study (the residual nucleus)

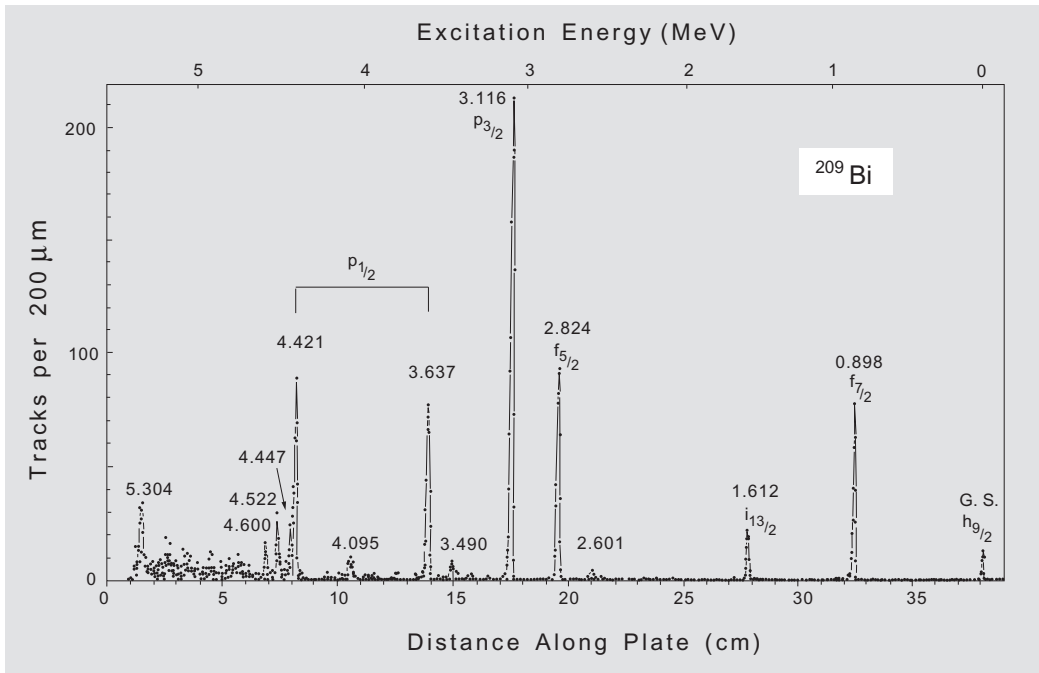


Figure 1.12: The spectrum of deuterons observed in the single-proton stripping reaction  $^{208}\text{Pb}(^3\text{He}, \text{d})^{209}\text{Bi}$  at an angle of  $110^\circ$  with respect to the  $^3\text{He}$  beam and at a bombarding energy of 18 MeV. The strong peaks correspond to particle states in  $^{209}\text{Bi}$  (cf. Figure 1.13). These are labelled by energy (in MeV) and the single-particle quantum numbers  $l$  and  $j$ . A significant “fragmentation” of the  $p_{1/2}$  independent-particle configuration is evident. The  $^{209}\text{Bi}$  ground state is on the right. Weak peaks in the spectrum are non-independent-particle states. (The figure is from Ellegaard C., Patnaik B. and Barnes P.D. (1970), *Phys. Rev. C* **2**, 2450.)

is  ${}^{209}_{83}\text{Bi}_{126}$ . The number of deuteron tracks per  $200\mu\text{m}$  in the photographic emulsion on the plate in the focal plane of the magnetic spectrometer is shown as a function of distance along the plate in centimetres. The distance along the plate is converted into energy by suitable calibration procedures. The nucleus  ${}^{209}_{83}\text{Bi}_{126}$  is considered to have a closed neutron shell and a closed proton shell plus one proton. Thus, it is expected to have a low-energy spectrum corresponding to the allowed single-particle states of a proton outside of the  $Z = 82$  closed proton shell. With this perspective in mind, the strong peaks in Figure 1.12 are associated with single-proton states and the weak peaks are associated with states which have a small component of a single-particle state mixed with a large component of other states; i.e., states in which the last proton is coupled to excited states of  ${}^{208}\text{Pb}$  (cf. Figures 1.13 and 1.52).

Low-energy states in odd-mass nuclei adjacent to  ${}^{208}\text{Pb}$  are shown in Figure 1.13. These states are single-particle states in  ${}^{209}\text{Bi}$  and  ${}^{209}\text{Pb}$ , and single-hole states in  ${}^{207}\text{Tl}$  and  ${}^{207}\text{Pb}$ . The nucleus  ${}^{209}\text{Bi}$  is discussed above. The neutron particle states in  ${}^{209}\text{Pb}$  can be identified using a single-neutron stripping reaction such as  ${}^{208}\text{Pb}(d, p){}^{209}\text{Pb}$ . Pickup reactions<sup>5</sup> such as  ${}^{208}\text{Pb}(d, t){}^{207}\text{Pb}$  and  ${}^{208}\text{Pb}(d, {}^3\text{He}){}^{207}\text{Tl}$  identify hole states. Some information is given also in Figure 1.13 on particle states in  ${}^{207}\text{Pb}$  and hole states in  ${}^{209}\text{Bi}$  and  ${}^{209}\text{Pb}$ . For example, proton hole states in  ${}^{209}\text{Bi}$  can be identified using the  ${}^{210}\text{Po}(t, \alpha){}^{209}\text{Bi}$  reaction (cf. Figure 1.23).

It is observed that only the ground state of  ${}^{208}\text{Pb}$  and the several single-particle and single-hole states in the  $A = 209$  and  $A = 207$  nuclei are reasonably described as independent-particle states. In particular, it is found that the excited states of  ${}^{208}\text{Pb}$  are not obtained simply by promoting a nucleon from an occupied to an unoccupied state, i.e., they are not simple one-particle-one-hole states. They are observed rather to be coherent linear combinations of one-particle-one-hole states. We shall have more to say about these states in Volume 2.

### 1.3.3 The shell model

The shell model is the basic microscopic model of nuclear structure theory. It is formulated on the premise that the nuclear Hamiltonian can be expressed as a sum of an independent-particle Hamiltonian and a residual interaction,  $\hat{V}$ , i.e.,

$$\hat{H} = \hat{H}_0 + \hat{V}. \quad (1.6)$$

The Hamiltonian  $\hat{H}_0$  is a sum of single-particle Hamiltonians,

$$\hat{H}_0 = \sum_{i=1}^A \hat{h}_i, \quad (1.7)$$

---

<sup>5</sup>We use the standard abbreviations:  $d \equiv {}^2_1\text{H}_1$ ,  $t \equiv {}^3_1\text{H}_2$ ,  $\alpha \equiv {}^4_2\text{He}_2$ .

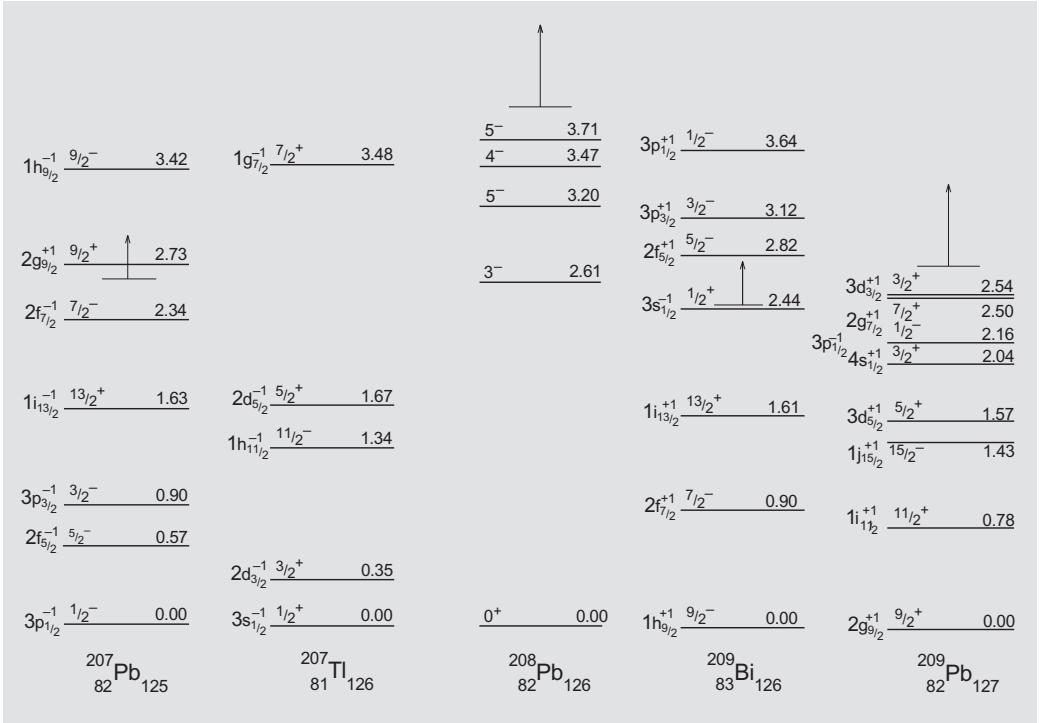


Figure 1.13: Low-energy states in odd-mass nuclei adjacent to  $^{208}\text{Pb}$ . Excitation energies are in MeV. Levels are labelled by their spin and parity  $J^{\pi}$  and, for the odd-mass nuclei, the single-particle quantum numbers  $n, l, j$  are given, together with their particle (+1) or hole (-1) character. Parity is given by  $(-1)^l$ , where  $l = 0, 1, 2, 3, 4, 5, 6, 7$  are labelled by s, p, d, f, g, h, i, j. The vertical arrows indicate the presence of higher energy excited states whose energies are known but are omitted from the figure. (The data are from *Nuclear Data Sheets*.)

where  $\hat{h}_i$  governs the motion of the  $i$ 'th nucleon. It corresponds to a system of nucleons moving independently in a spherically symmetric field, commonly referred to as the *single-particle potential*. The single-particle potential is chosen to represent the average interaction of a nucleon with the other nucleons.

In principle the nuclear Hamiltonian can always be expressed as a sum of two terms as in Equation (1.6). But, such an expression is only useful if  $\hat{H}_0$  exhibits a shell structure and if the residual interaction is not so strong that it destroys this structure.

A simple single-particle Hamiltonian,  $\hat{h}_i$ , is of the form

$$\hat{h}_i = \frac{\hat{p}_i^2}{2M} + U(r_i), \tag{1.8}$$

where  $\hat{\mathbf{p}}_i$  ( $= -i\hbar\nabla_i$ ) is the momentum of the  $i$ 'th nucleon, so that  $\hat{p}_i^2 = \hat{\mathbf{p}}_i \cdot \hat{\mathbf{p}}_i = -\hbar^2\nabla^2$ ,  $M$  is the mass of a nucleon,  $\mathbf{r}_i$  is its position vector ( $r_i = |\mathbf{r}_i|$ ), and  $U$  is a

potential for a central single-particle field. Because all neutrons are identical and all protons are identical, the Hamiltonian  $\hat{h}_i$  can only depend on the nucleon to the extent of distinguishing between neutrons and protons. Thus, for simplicity we shall drop the subscript on  $\hat{h}_i$  and write

$$\hat{h} = \frac{\hat{p}^2}{2M} + U(r). \quad (1.9)$$

However, it is to be understood that the potential  $U$  may be different for neutrons and protons. Indeed, a repulsive Coulomb potential should be added for protons.

Because nuclear forces are of short range compared to the dimensions of a nucleus, a natural choice of single-particle potential is one of the form

$$U(r) = -V_0\rho(r), \quad (1.10)$$

where  $\rho$  is the nuclear density (cf. Figures 1.6 and 1.7). To the extent that the density distribution of a nucleus resembles that of a liquid drop, we might consider the finite square-well potential,

$$U(r) = \begin{cases} -V_0 & \text{if } r < R, \\ 0 & \text{if } r \geq R. \end{cases} \quad (1.11)$$

A more realistic single-particle potential, proportional to the density distribution given by Equation (1.3), is the Woods-Saxon potential<sup>6</sup>

$$U(r) = -V_0 \left\{ 1 + \exp\left(\frac{r-R}{a}\right) \right\}^{-1}. \quad (1.12)$$

The disadvantage of these potentials is that single-particle wave functions have to be computed numerically.

There are two potentials which provide single-nucleon wave functions in analytic form: the spherical harmonic oscillator

$$U(r) = \frac{1}{2}M\omega^2r^2 + \text{const.} \quad (1.13)$$

and the infinite square-well potential,

$$U(r) = \begin{cases} -V_0 & \text{if } r < R, \\ \infty & \text{if } r \geq R. \end{cases} \quad (1.14)$$

These two potentials and the Woods-Saxon potential are illustrated in Figure 1.14. The most commonly used potential is that of the spherical harmonic oscillator.

It can be seen from Figure 1.14 that the harmonic oscillator potential has some resemblance to the Woods-Saxon potential in the interior regions of the nucleus but it goes to infinity with increasing radius. The large-radius behaviour of the harmonic oscillator is less of a problem than it would appear to be at first sight because nuclear wave functions, for bound nucleons, fall off rapidly and approach

<sup>6</sup>Woods R.D. and Saxon D.S. (1954), *Phys. Rev.* **95**, 577.

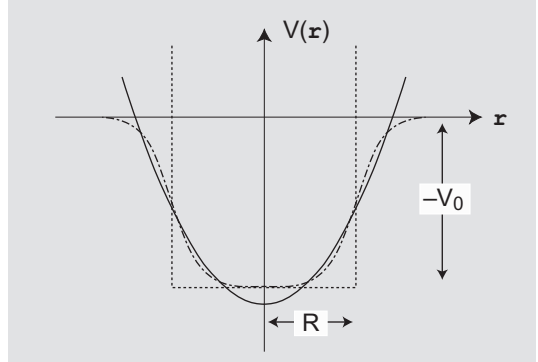


Figure 1.14: Single-particle shell-model potentials: an infinite square well potential (dashed line); a Woods-Saxon potential (dot-dashed line); and a harmonic oscillator potential (solid line).

zero at large radii. They simply fall off more rapidly in the oscillator potential than they would in a more realistic potential. Thus, a harmonic oscillator potential is not as realistic as a Woods-Saxon potential. But, with a little adjustment, it gives similar results. The reason for its popularity is that its wave functions and energy levels have analytical expressions. We shall also find, in subsequent chapters, that the harmonic oscillator shell model has many symmetries and provides a useful basis for the expression of collective models with a microscopic interpretation.

The spatial wave functions for a single particle in a spherically symmetric potential can be expressed in spherical polar coordinates in the form

$$\psi_{nlm}(r, \theta, \varphi) = R_{nl}(r)Y_{lm}(\theta, \varphi), \tag{1.15}$$

where  $n$  is a radial quantum number,  $Y_{lm}$  is a spherical harmonic, and  $l, m$  are orbital angular momentum quantum numbers. These quantum numbers take values in the ranges  $n = 1, 2, 3, \dots$ ,  $l = 0, 1, 2, \dots$  and  $m = -l, \dots, +l$ , respectively. Intrinsic spin degrees of freedom are suppressed for the moment but will be included shortly. Because a spherically symmetric potential is rotationally invariant, the single-particle energies,  $\epsilon_{nl}$ , depend on  $n$  and  $l$  but not on  $m$ . The parity of a single-particle wave function  $\psi_{nlm}$  is  $(-1)^l$ ; this follows from the symmetry of the spherical harmonics,  $Y_{lm}(\theta, \varphi)$ , under inversion.

For a spherical harmonic oscillator, cf. Section 5.8, the energy levels are given by

$$\epsilon_{nl} = (N + 3/2)\hbar\omega, \tag{1.16}$$

where  $N$  (not to be confused with the neutron number) is given by

$$N = 2(n - 1) + l. \tag{1.17}$$

These energies are shown in Figure 1.15. For each value of  $l$ , the quantum number  $m$  takes  $2l + 1$  values. With two spin states for a nucleon (spin up and spin down), one finds that the multiplicity of states at each level is equal to  $(N + 1)(N + 2)$ . Because of the Pauli exclusion principle, no two identical nucleons in a nucleus can

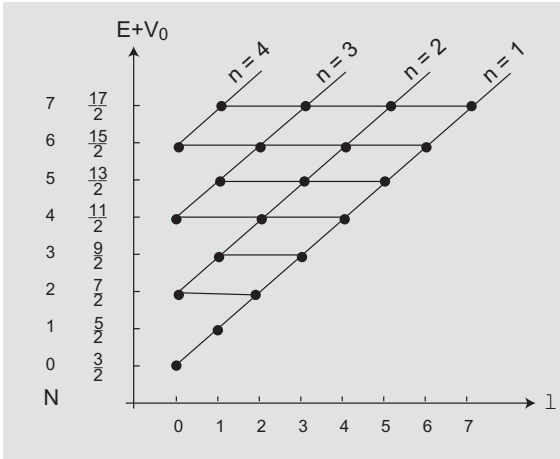


Figure 1.15: The energy eigenvalues of a spherical harmonic oscillator (cf. Equations (1.16) and (1.17)). Note the degeneracy in  $l$ . The energies are given in units of  $\hbar\omega$ .

have the same single-particle wave function. Thus, with harmonic oscillator wave functions, at most  $(N+1)(N+2)$  neutrons and  $(N+1)(N+2)$  protons can occupy the single-particle states of the  $N$ 'th level. This number is called the *occupancy* of the level. If one adds the single-particle occupancies, starting from the bottom, to find the numbers of neutrons and protons required to fill succeeding harmonic oscillator shells, one finds closed shells when the neutron and proton numbers take the values 2, 8, 20, 40, 70, 112, 168, ... The first few of these numbers correspond to experimentally observed magic numbers.

The frequency,  $\omega$ , of the harmonic oscillator potential, appropriate for a shell model description of an  $A$ -nucleon nucleus, is naturally chosen such that the mean-square radius of the nucleus, in its harmonic-oscillator ground state will accord with the measured value as shown, for a few nuclei, in Figure 1.5. By such means it is determined (cf. Exercise 5.32) that an appropriate choice is given by the formula

$$\hbar\omega \approx 41A^{-1/3} \text{ MeV}. \quad (1.18)$$

The energy levels for a particle in a finite square-well potential are easily determined; however, to obtain meaningful results, it is necessary to allow the radius of the potential to become progressively larger as the single-particle states are filled and the nucleus becomes bigger. The relationship between nuclear radius and nucleon number is given by Equations (1.1) and (1.2). For the spherical harmonic oscillator, the changing dimensions of the potential simply change the  $\hbar\omega$  unit of energy and a corresponding unit of length; i.e., the energies and wave functions can all be expressed in dimensionless units which are simultaneously valid for all nuclei. This cannot be done for a finite potential. But, it can be done for an infinite square-well potential. The energy levels for a particle in an infinite isotropic square well of radius  $R$  are shown in Figure 1.16. The notable feature of the results is that the single-particle states of constant  $N = 2(n-1) + l$  are no longer degenerate, as

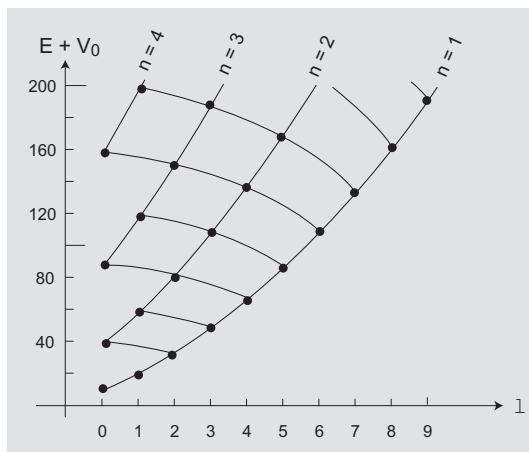


Figure 1.16: The energy eigenvalues of a particle in an infinite isotropic square well. The energies are given in units of  $\hbar^2/2MR^2$ . Compare the pattern as a function of angular momentum with that of Figure 1.15.

they are in the harmonic oscillator, but decrease in energy as  $l$  increases. Again there are gaps in the energy level spectrum. Moreover, the successive filling of the single-particle levels leads to shell closures at  $N, Z = 2, 8, 20, 34, 58, 92, 138, 186, \dots$ . As for the spherical harmonic oscillator potential, the first few of these numbers correspond to the experimental magic numbers.

To obtain the full sequence of magic numbers, it is necessary to include a strong *spin-orbit interaction* in the single-particle Hamiltonian. This important breakthrough in the development of the shell model was discovered independently by Goeppert-Mayer<sup>7</sup> and by Haxel, Jensen, and Suess.<sup>8</sup> Further, as noted by Nilsson,<sup>9</sup> one can simultaneously retain the primary advantage of the spherical harmonic oscillator, of giving analytical results, while simulating the effects of a more realistic, more square-shaped potential. All one has to do is add a term  $DI^2$  to the oscillator potential. The  $l$  degeneracy (cf. Figure 1.15) is then broken and, with  $D < 0$ , the energy of a state of angular momentum  $l$  is lowered by an amount proportional to  $l(l+1)$ . With a suitable value of  $D$ , this produces a pattern of single-particle energies similar to that shown for the infinite square-well potential in Figure 1.16, i.e., the  $l^2$  term effectively interpolates between the oscillator and the infinite square-well. Physically, the recipe is sensible; higher  $l$  values have larger average orbital radii because of the centrifugal potential. Thus, a “flatter” potential, such as the square-well potential, results in lower energies for higher  $l$  states. With some adjustment of the value of  $D$  and the inclusion of a spin-orbit interaction, one can get analytical expressions for single-particle energies which reproduce the observed magic numbers.

Following Goeppert-Mayer, Jensen *et al.*, and Nilsson, we consider a single-

<sup>7</sup>Goeppert-Mayer M. (1949), *Phys. Rev.* **75**, 1969.

<sup>8</sup>Haxel O., Jensen J.H.D. and Suess H.E. (1949), *Phys. Rev.* **75**, 1766.

<sup>9</sup>Nilsson S.G. (1955), *Mat. Fys. Medd. Dan. Vid. Selsk.* **29** (16).

particle Hamiltonian

$$\hat{h} := \frac{\hat{p}^2}{2M} + \frac{1}{2}M\omega^2 r^2 + D\hat{\mathbf{I}}^2 + \xi \hat{\mathbf{I}} \cdot \hat{\mathbf{s}}, \quad (1.19)$$

where  $\hat{\mathbf{I}}$  is the orbital angular momentum and  $\hat{\mathbf{s}}$  is the intrinsic spin of the nucleon. Empirically,  $\xi < 0$  and, as already noted,  $D < 0$ . With the inclusion of intrinsic spin, the total angular momentum of a nucleon of orbital angular momentum  $l$  takes one or other of the values  $j = l \pm 1/2$ . With the identity

$$\hat{\mathbf{I}} \cdot \hat{\mathbf{s}} = \frac{1}{2}(\hat{\mathbf{j}}^2 - \hat{\mathbf{I}}^2 - \hat{\mathbf{s}}^2), \quad (1.20)$$

we see that the  $\hat{\mathbf{I}} \cdot \hat{\mathbf{s}}$  operator has eigenvalues given by

$$\hat{\mathbf{I}} \cdot \hat{\mathbf{s}} \psi_{nljm} = \begin{cases} \frac{1}{2}l \psi_{nljm} & \text{for } j = l + 1/2, \\ -\frac{1}{2}(l+1) \psi_{nljm} & \text{for } j = l - 1/2. \end{cases} \quad (1.21)$$

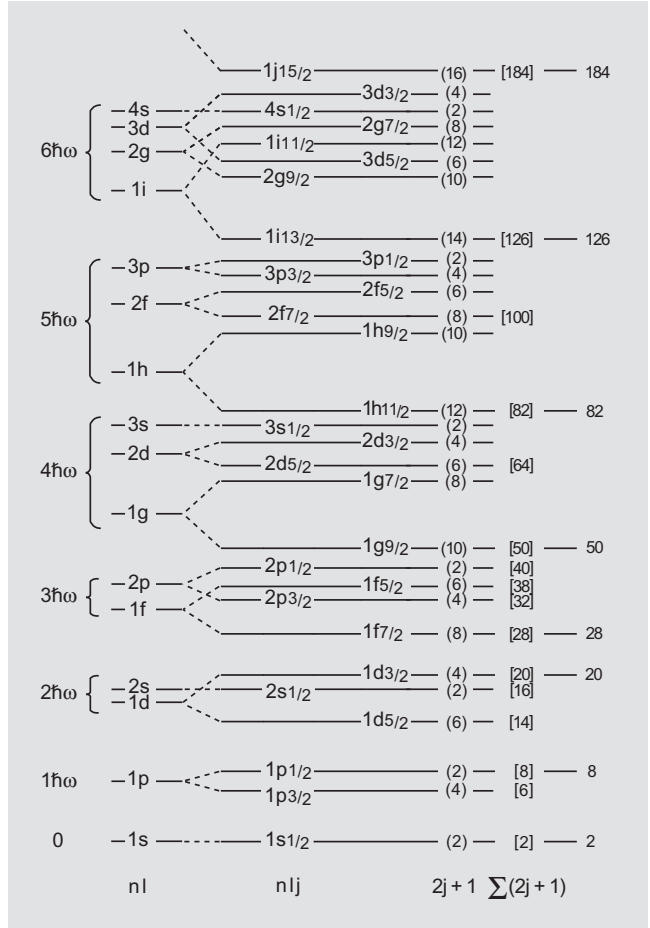
The single-particle energy level sequence for a Hamiltonian of the type given by Equation (1.19) is shown in Figure 1.17. Each level now has an occupancy equal to  $(2j+1)$ . The figure shows these occupancies and the cumulative occupancies at the energy gaps, corresponding to the nucleon numbers which close a shell. It can be seen that these numbers are now the experimentally observed magic numbers.

Support for the independent-particle structure underlying nuclei in the  $^{208}\text{Pb}$  region is provided by a comparison of electron scattering from  $^{205}\text{Tl}$  and  $^{206}\text{Pb}$ . These nuclei differ by a proton in the  $3s_{1/2}$  shell-model orbit. The differences between elastic electron scattering from  $^{205}\text{Tl}$  and  $^{206}\text{Pb}$  reflect the density distribution of a proton in the  $3s_{1/2}$  orbital. The density distribution deduced in this way is shown in Figure 1.18. The number of radial nodes agrees with the shell model radial quantum number.

The detailed properties of states in odd-mass nuclei adjacent to doubly-closed shells show that the independent-particle nature of these states is only approximate; there are observable correlation effects induced by the residual interaction,  $V$ , of Equation (1.6). For example, the ground state of  $^{17}\text{O}_9$  (cf. Figure 1.19) has a non-zero electric quadrupole moment. This would be impossible if the ground state of  $^{16}\text{O}$  were a pure closed-shell-plus-single-neutron configuration because the  $^{16}\text{O}$  core has zero quadrupole moment and neutrons have no electrical charge. Thus, the non-zero quadrupole moment implies the presence of correlations between the extra-core neutron and the core. The nature of these correlations is easily understood in terms of *core polarization*. The effect is illustrated schematically in Figure 1.20 which shows the density distribution of the  $^{16}\text{O}$  core pulled out of its spherical shape by the attractive forces of the extra-core neutron. The effect of the extra-core neutron on the core resembles the tidal motions of the Earth's oceans caused by the Moon's gravitational attraction.

A predominantly single-particle state, perturbed by small admixtures of non-single-particle configurations, is sometimes described as a *dressed* single-particle

Figure 1.17: The energy-level sequence for a single particle moving in a spherical (isotropic three-dimensional) harmonic oscillator potential with well-flattening and spin-orbit coupling terms. The levels are labelled by the radial ( $n$ ), orbital angular momentum ( $l$ ), and total spin ( $j = l \pm \frac{1}{2}$ ), quantum numbers; states with  $l = 0, 1, 2, 3, \dots$  are labelled  $s, p, d, f, \dots$ . The maximum particle occupancies,  $2j + 1$ , of the subshells are given in parenthesis and the cumulative particle numbers are given in square brackets. The  $\hat{I}^2$  term removes the angular momentum degeneracy of each major shell. The  $\hat{I} \cdot \hat{s}$  term produces the shell gaps at the empirically established numbers 2, 8, 20, 28, 50, 82, 126 (184 has not yet been reached). There are separate such diagrams for protons and for neutrons. (The figure is based on a figure in Mayer M.G. and Jensen J.H.D. (1955), *Elementary Theory of Nuclear Shell Structure* (Wiley, New York), p. 58.)



state. This useful concept leads to the idea of *renormalised* or *effective* single-particle parameters. For example, both the ground-state electric quadrupole moment and the electric quadrupole transition rate between the ground state and first excited state in  $^{17}\text{O}$  (cf. Figure 1.19) can be described within the framework of the independent-particle model if the odd neutron is given a nonzero effective charge. Using a single-particle model for the extra-core neutron and giving it an effective charge (equal to 43% of the proton charge) provides a consistent description of the electric quadrupole properties of  $^{17}\text{O}$ .

The mixing of single-particle states with more complicated shell-model configurations is a relatively simple renormalisation effect in closed-shell-plus-one nuclei. This is because the more complicated configurations, to which the single-particle states couple, have considerably higher unperturbed energies relative to the independent-particle Hamiltonian  $H_0$ .

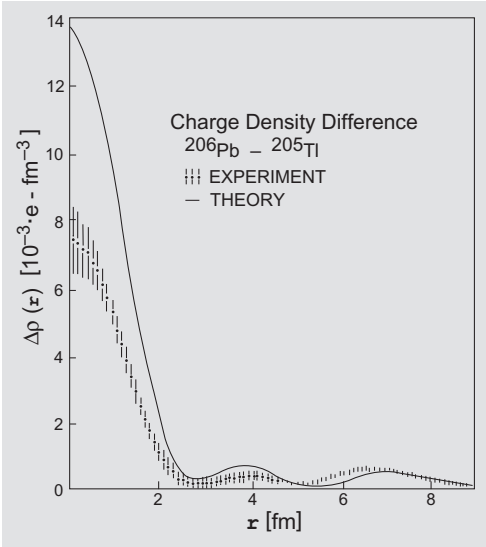


Figure 1.18: The charge density difference between  $^{206}\text{Pb}$  and  $^{205}\text{Tl}$  determined by elastic electron scattering. The nuclei  $^{206}\text{Pb}$  and  $^{205}\text{Tl}$  differ, according to the single-particle model, by a proton in the  $3s_{1/2}$  orbital (cf. Figure 1.13). This is reflected in the figure by the two minima in  $\Delta\rho(r)$  at 2.8 fm and 5.2 fm corresponding to the two radial nodes expected for an  $n = 3$  orbital. (The figure is taken from Celenza L.S., Harindranath A. and Shakin C.M. (1985), *Phys. Rev. C* **32**, 2173.)

$1/2^+$	0.87	$\tau$ ( $E2; 1/2^+ \rightarrow 5/2^+$ )	$258.6 \pm 2.6$ ps	260 ps (norm)
$5/2^+$	0	$Q$ ( $5/2^+$ )	$-2.58 \pm 0.05$ efm <sup>2</sup>	$-2.8$ efm <sup>2</sup>
$^{17}\text{O}$		experiment	theory	( $e_{\text{eff}} = 0.43e$ )

Figure 1.19: Some properties of the ground state and first excited state of  $^{17}\text{O}$ . The ground state has spin-parity  $5/2^+$  and an electric quadrupole moment of  $-2.58$  efm<sup>2</sup>. The first excited state at 0.87 MeV has spin-parity  $1/2^+$  and a mean lifetime of 258.6 ps. This mean lifetime reflects the rate of the electric quadrupole transition to the ground state. (The data are taken from Tilley D.R., Weller H.R. and Cheves C.M. (1993), *Nucl. Phys. A* **564**, 1.)

For nuclei having several valence-shell nucleons, there are generally many configurations with similar unperturbed energies. The residual interaction,  $\hat{V}$  (cf. Equation (1.6)), then results in a large mixing of states and far more dramatic effects than simply the renormalisation of independent-particle model properties. Indeed, large correlations of various kinds emerge corresponding to different collective phenomena; such correlations are the subject of this book. Particularly prevalent in singly-closed shell nuclei are the so-called *pairing correlations*.

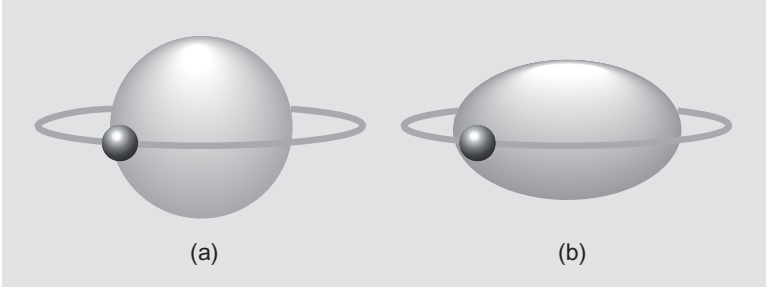


Figure 1.20: Schematic illustration of the  $^{17}\text{O}$  nucleus as a neutron coupled to an  $^{16}\text{O}$  core. If the  $^{16}\text{O}$  core were spherical, as in (a), then, since the neutron has no charge, the  $^{17}\text{O}$  nucleus would have zero quadrupole moment. However, if the neutron polarizes the core, as in (b), then  $^{17}\text{O}$  can acquire a non-zero quadrupole moment corresponding to an oblate shape.

### Exercises

- 1.6** Use Figure 1.18 and the wave function for a  $3s_{1/2}$  harmonic oscillator radial wave function (cf. Equation (1.15)),

$$R_{3s_{1/2}}(r) \sim [4(\alpha r)^2 - 20(\alpha r) + 15]e^{-\alpha^2 r^2/2}, \quad (1.22)$$

where  $\alpha = \sqrt{m\omega/\hbar}$  and  $m_p = 1.67 \times 10^{-27}$  kg, to estimate  $\hbar\omega$  for a harmonic oscillator potential.

- 1.7** Normalise the  $3s_{1/2}$  wave function (given in Exercise 1.6) on the interval  $0 \leq r < \infty$ , and calculate  $\langle r^2 \rangle$  for this single-particle state in  $^{206}\text{Pb}$  [recall that, for a normalised radial wave function,  $\int_0^\infty [R_{nl}(r)]^2 r^2 dr = 1$ ].
- 1.8** Construct a shell model energy level diagram using  $\hbar\omega$  from Exercise 1.6,  $D = -0.5$  MeV and  $\xi = -0.5$  MeV.
- 1.9** Derive Equation (1.21) from Equation (1.20).

### 1.4 Pairing in nuclei

Pairing in nuclei is the coupling of nucleons in pairs to states of zero angular momentum. The phenomenon is most evident in nuclei with two neutrons or two protons outside of doubly-closed shells. However, it occurs to some extent in all nuclei and is responsible for the fact that all even-even nuclei have zero angular momentum ( $J = 0$ ) ground states.

The tendency of spin- $1/2$  particles to form  $J = 0$  coupled pairs is well-known in a variety of many-fermion systems. For example, it is believed to be responsible for superconductivity<sup>10,11,12,13</sup> in macroscopic condensed systems. In this case, the

<sup>10</sup>Cooper L.N. (1956), *Phys. Rev.* **104**, 1189.

<sup>11</sup>Bardeen J., Cooper L.N. and Schrieffer J.R. (1957), *Phys. Rev.* **108**, 1175.

<sup>12</sup>Bogolyubov N.N. (1958), *Nuovo Cimento* **7**, 794.

<sup>13</sup>Bogolyubov N.N. (1959), *Sov. Phys.-Uspekhi* **2**, 236.